In-situ Study of Structure Formation Under Stress in Stretchable Conducting Nanocomposites

Debmalya Roy,[a,b] Vaishnav B[c], Sarathlal Koyiloth Vayalil,[c] Ajay Gupta,[c] N. Eswara Prasad,[a] Benedikt Sochor,[d] Matthias Schwartzkopf,[d] Stephan V. Roth,[d,e] Tobias Kraus, [b,f*]

[a.] DMSRDE, GT Road, Kanpur-208013, India

[b.] INM – Leibniz-Institute for New Materials, Campus D2 2, 66123, Saarbrücken, Germany

[c.] UPES, Bidholi, Dehradun-248007, India

[d.] Deutsches Elektronen-Synchrotron DESY, Notkestrasse 85, 22607, Hamburg, Germany

[e.] Division of Coating Technology, KTH Royal Institute of Technology, Teknikringen 48, Stockholm, 100 44, Stockholm, Sweden

[f] Colloid and Interface Chemistry, Saarland University, 66123, Saarbrücken, Germany

* *Corresponding Author: Email: tobias.kraus@leibniz-inm.de*

Abstract:

One of the major limitations of flexible sensors is the loss of conductivity by multiple stretching and bending. Conducting fillers with two different geometries, carbon black and carbon nanotubes, were introduced in polydimethylsiloxane (PDMS) for physical insights into the structure formation of nanofillers by application of periodic tensile stress. The loading of nanofillers was selected beyond the percolation threshold to determine the cyclic stability of the resulting network channels. The surface chemistry of carbon nanotubes has been varied to understand the interfacial interactions at length scale. The combination of *in-situ* stretching, annealing, and vis-à-vis conductometry of nanocomposite films with synchrotron–based ultra-small angle X-ray scattering experiments, enable us to highlight the importance of fractal dimensions of nanofillers for the molecular level interactions. The irreversible formation of nanofiller network geometries under cyclic stress and annealing were found to be responsible for electrical properties of flexible conducting film.

Table of Contents Graphic:

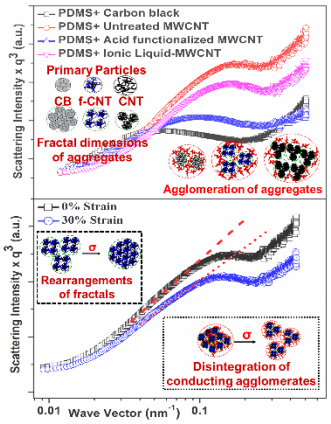

Keywords:

Conducting nanofillers; stretchable conductors; elastomer matrix; cyclic stress; scattering from aggregates

The development of stretchable conducting materials with high cyclic stability is one of the challenges in materials science and engineering when fabricating flexible wearable sensors.[1,2] Elastic conductors enable the physiological sensors to be printed on any arbitrary locations and any substrate geometry. This is an important step towards producing intelligent surfaces for human-machine interfaces.[3,4] Printable physiological sensors on human skin or textile surface have huge application potential in healthcare, energy as well as strategic areas and has been an intense research topic across the world.[5,6] The conducting nanofillers produce interpenetrating network structures to make the elastomeric matrix conducting whereas the chemistry of nanomaterial decides the cyclic stabilities of the conduction channels upon stretching/bending.[7]

The challenges and opportunities of producing conduction channels with carbon black have been studied in detail to achieve their percolation thresholds. However, it has been reported that a nanomaterial loading way beyond the percolation threshold is required for generating robust conduction networks during high degree of sustained applied stress.[8-10] The chemical and rheological properties of conducting particles and elastomers have been the key design criteria

for printing inks to optimize the screen printing's fluid dynamics and sustained conductivity with strain. Carbon based nanofillers have greater application potential than metals for making high performance inks due to their lower price, better flexibility and lower percolation threshold where the ink's effectiveness is primarily limited by high particle agglomeration due to particle-particle interactions.[11-13] However, there are still opportunities remaining to improve the ink formulation addressing the challenges of nanofillers dispersion, ink rheology and interpenetrating network patterns formation under cyclic stress.

We have extended our study beyond the filler percolation threshold to examine the role of particle-particle and particle-matrix interactions on the viscoelastic properties of nanocomposites.[14] We have observed the reduction of conductivity in successive stretching and release of stress in carbon nanoparticles based PDMS film even at a higher filler loading beyond the percolation threshold (Figure 1(a)). To understand the correlation between structure formation and conductivity of carbon black nanocomposite by the application of stress, a combined synchrotron based ultra-small angle X-ray scattering (USAXS) and in-situ conductivity measurements during mechanical stretching in a controlled way have been carried out. USAXS is a non-destructive method to characterize structures with dimensions from a few microns to nanometre length scales.

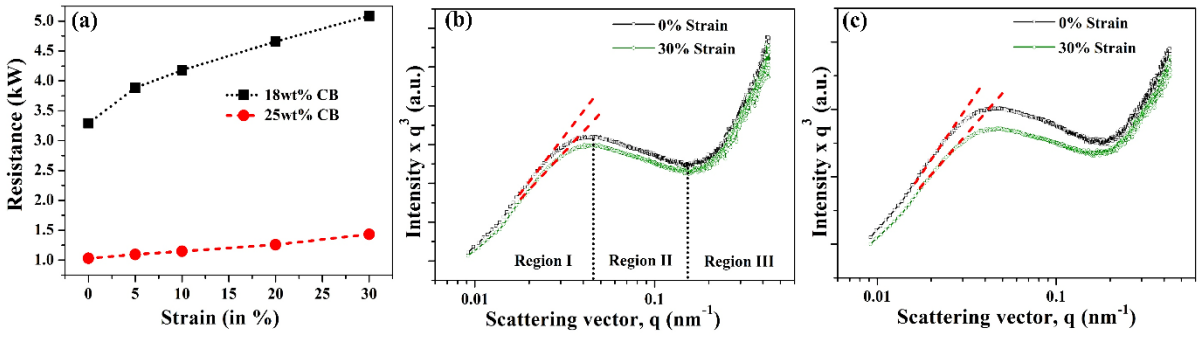

Figure 1: The resistance values (a) of PDMS nanocomposite films with 18 wt% (black) and 25 wt% (red) of carbon black (CB) where figure (b) and (c) represent the small angle scattering data for 0% (black) and 30% (green) stretched films of 18 and 25 weight fractions CB samples.

It has been reported that the agglomeration of basic filler particles in polymer matrix generates aggregates with wide size distributions.[15] Further, these aggregates act as the basic units for the formation of larger sized agglomerates and in this way, the structures with different length scales have been formed.[16-17] In order to describe such a system with different hierarchical levels, the concept of fractals dimensions has been introduced. Mass fractal dimension d_m, which denotes branching of the clusters can be defined in terms of radius of gyration r_g as

$$N \propto \left(\frac{r_g}{d}\right)^{d_m} \qquad \text{------ (1)}$$

where N denotes the number of primary particles per aggregates and d denotes primary particle diameter. A low value of d_m corresponds to the minimum branched structure. The Monte Carlo simulation studies have carried out to highlight that r_g is a key factor in determining the percolation threshold in case of conducting carbon black.[16] It has been reported that the percolation threshold decreases with increasing values of radius of gyration which indicates larger sized clusters cause lower percolation threshold values. The scattering from fractal structures follows the power law decay of scattering intensity with the wave vector, and it can be further sub-divided into scattering from different length scale.[16,18] One can write the scattered intensity from mass fractal of size smaller than R_m as

$$I \propto \left(\frac{R_m}{q}\right)^{d_m} \qquad \text{------ (2)}$$

For a linear object, the value of d_m is 1, and for a homogeneous sphere it is considered as 3. Since in our case, the scattering from all hierarchical levels is exhibiting a decay exponent close to -3, we have thus multiplied our scattering intensities I by q^3 to emphasis scattering from different length scale structures. Figure 1(b) & figure 1(c) represent the *in situ* USAXS data of PDMS nanocomposite films under mechanical stretching with different CB weight percentages. We report strains of 0% and 30% in USAXS for the two different weight fractions of 18% (percolation threshold) and 25% of CB in the PDMS matrix, far above the percolation threshold.[14] The three different regimes have been identified in the figure, viz, smaller wave

vector regime with positive slope (region I) which represents aggregate mass fractal. The regime of negative slope (middle part, region II) corresponds to the surface fractal of primary particles, whereas larger wave vector regime (region III) has been assigned to internal structure of primary particles.[16]

The scattering at region II part (Figure 1(b), q range 0.05-0.15 nm^{-1}) is corresponding to structures with length scale roughly between 41 nm to 136 nm, which agrees well with the size of primary carbon black particles.[16,19] In the case of CB above the percolation threshold, both region II and region III are not varying significantly with stretching. It indicates that almost no variation in primary particle dimension and internal structure of particles with stretching. However, a clear variation in slope has been observed in Region I with stretching where the slope corresponding to a higher percentage of stretching is getting less steep as compared to the unstretched stage. We have observed the systematic decrease in slope with increased degree of stretching which indicates an increase in the fractal dimension. It may not be feasible to quantitatively evaluate the fractal dimension due to high polydispersity of the agglomerates. In both 18% and 25% CB samples, the resistance of the nanocomposite increases systematically with increasing percentage of stretching. At the same time, the volume fractal dimension of agglomerates also exhibits a systematic increase, as evidenced by a decrease in the slope of the curve in region I. The conductivity of 25% CB sample is found to be significantly higher as compared to the 18% CB which can be explained by the increase in slope with enhanced CB contents at region I. No change in slope is observed at region II and region III with increase in CB contents, however, the q range of region II differs with higher weight percentages of CB.

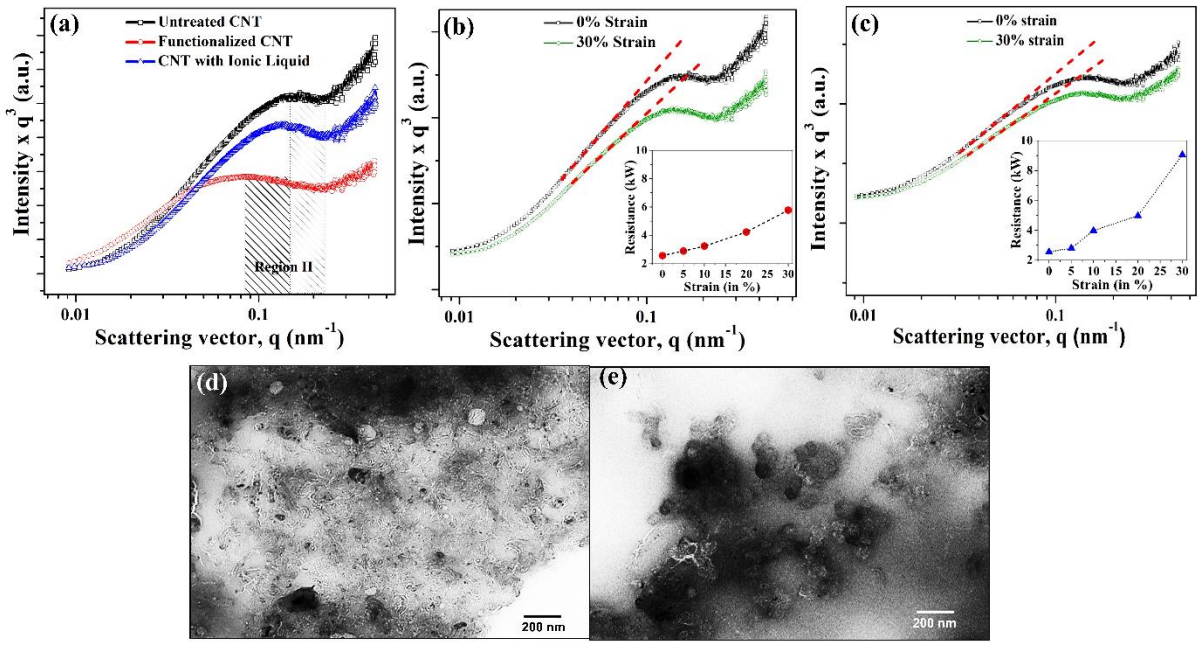

Figure 2. (a) represents the comparative USAXS data of PDMS films with 18 weight percentages of untreated MWCNTs (black), MWCNTs mixed with ionic liquid (blue) and nanotubes treated with acids (red). (b) and (c) are illustrating the scattering data for 0% (black) and 30% (green) stretched films of 18 and 25 weight fractions acid treated MWCNTs samples where the *in-situ* change in resistance of the film as a function of stretching is shown in the inset of the graph. The corresponding TEM images of the same lower (d) and higher (e) weight percentage cryo-ultramicrotomed nanotube samples were represented.

It has been reported that percolation threshold can be achieved at much lower loading with high aspect ratio nanofillers like carbon nanotubes.[8,20] We thus extended our study to 1D nanofillers filler like carbon nanotube, which has been considered as flexible rod like geometry.[21] It has been established that conducting properties beyond the percolation threshold of 1D nanofillers reinforced composites follows the similar trend as 0D fillers which may be explained by Doi-Edwards model of reptation of rod-like particle system.[22] A marginal reduction in the resistance was found when the MWCNT loading were increased from 18 to 25 weight percentages and contrary to carbon black the change in resistance by stretching was found to be much more significant at higher loading in 1D nanofillers. The TEM images (Figure 2) indicates that

untreated-MWCNTs are difficult to disperse in PDMS at higher loading which helps the growth of primary and secondary aggregates in polymer matrix composite. The cryo ultramicrotomy using Leica EM FC6 instrument of TEM samples at -1800C which is below the glass transition temperature of PDMS, ensured the retention of microstructural information in TEM study.

We have varied the surface chemistry of pristine MWCNTs by covalent functionalization (acid functionalized CNT)[23] and non-covalent functionalization (ionic liquid coated CNTs) to understand the cluster formation mechanism as a function of intramolecular interactions of CNT clusters and interfacial interactions with polymer matrix. USAXS scattering profile of $I \times q^3$ *vs* q for CNTs of same weight percentage with different functionalized surfaces are shown in figure 2(a). It is to be noted that, when we compare q values corresponding to the crossover point between region I and region II for pristine and acid functionalized nanocomposite samples, one could see a clear shift towards lower q values for acid functionalized ones. This indicates variation in aggregates and agglomerates size due to functionalization which is evident from TEM images at different weight fractions of nanofillers loading [Figure. 2]. The regimes of the scattering graph have unique power law fits where the exponents (slopes) are the characteristic of scatterer's dimension, which can be obtained from the corresponding q values. The different regions of scattering vector were attributed to the different mass fractals of the nanofillers which have been discussed in detailed in the previous report[16]. The change in slope is distinct in the region I of the scattering plot and thus the change in slopes in that region have been quantified and tabulated in Table 1.

Table 1. The slope of the curves in region I of the scattering curve which are the indicative of fractal dimension, has been obtained through the apparent linear fitting. The linear fit has been carried out in the characteristic region where the curve possesses considerable linearity (lesser error). The obtained values of the slopes are as tabulated.

Figure number	Strain (%)	Slope	% Change in slope
1b	0	0.5236	2.29
	30	0.5116	
1c	0	0.6200	2.47
	30	0.6047	
2b	0	0.5412	2.03
	30	0.5302	
2c	0	0.5761	2.04
	30	0.5643	
3a	0	0.5679	2.75
	30	0.5523	
3b	0	0.4429	1.69
	30	0.4354	

In region II of figure 2(a), the *q* range for pristine CNTs is 0.15 nm^{-1} to 0.21 nm^{-1} which corresponds to primary particle sizes of 42 nm to 29 nm, while for acid functionalized CNTs, it is 0.08 nm^{-1} to 0.21 nm^{-1}, corresponding to size range of 79 nm to 30 nm. Thus, the mean value of the size distribution of aggregates and agglomerates are found to be larger for acid functionalized samples as compared to pristine and ionic liquid ones. This could be explained in terms of variation in nanotube length upon acid functionalization along with the attribution of intermolecular interactions between individual functionalized nanotubes and this could be responsible for the differential cluster formations in polymeric matrix.[24] The scattering intensity at very low *q* regime is also high for acid functionalized CNT samples. The slope of the region I of the graph is found to be decreasing with different surface treated nanotube samples which were determined from the linear fitting of the slope (Table 1). In the case of acid functionalized CNT samples, the slope has been changed drastically as compared to the pristine and the ionic liquid-based samples, indicating the increase in fractal dimensions. By comparing the different surface treated MWCNTs, we can conclude that fractal dimension of CNT aggregates is lowest

when CNT surface is not passivated which can be understood by the π- π interactions with PDMS chains with further ramified the fractal dimension of unmodified CNT in PDMS matrix.[25] It is to be noted that at 18 wt% both covalent and non-covalent modified CNTs are much below their percolation thresholds.

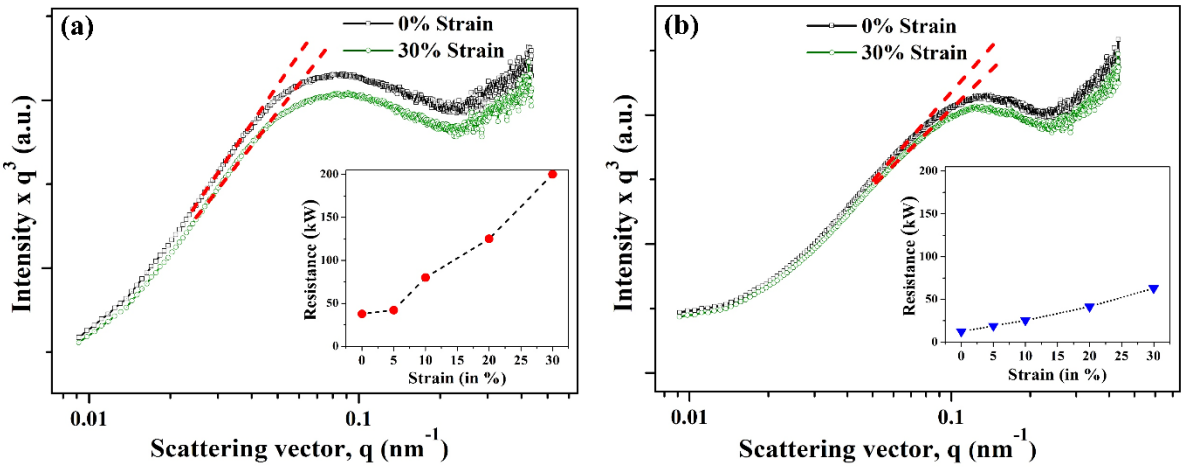

Figure 3: (a) and (b) are exhibiting the USAXS data for 0% (black) and 30% (green) stretched films of 30 wt% acid treated MWCNTs samples and MWCNT mixed with ionic liquid respectively where the *in-situ* change in resistance of the film as a function of stretching is shown in the inset of the graph.

In-situ USAXS studies have then been carried out during stretching of pristine CNT samples with two different weight percentages 18% and 25% in PDMS matrix and are shown in figure 2(b) and 2(c) respectively. Resistance of the films were measured simultaneously during stretching and are shown in the insets of figure 2(b) and 2(c) for respective weight fraction of samples. In both cases, resistance is found to be increasing with increasing percentage of stretching as similar to CB samples. The lower q regime of $I \times q^3$ *vs* q scattering data shows a decrease in slope (Table 1) with increasing stretching which indicates the variation in fractal dimensions of aggregates and agglomerates. It supports our earlier observation that fractal dimension is increasing with stretching. No pronounced variation in slope is observed with stretching in the region II corresponding to primary particle dimensions. Similar to CB samples,

high polydispersity of aggregates in CNT systems prevents us from calculating quantitative estimation of fractal dimensions at different length scales. $I \times q^3$ *vs* q plot corresponding to *in-situ* USAXS measurements during stretching for acid functionalized systems are shown in figure 3(a) and 3(b). The conductivity data have been placed in the insets of figure 3(a) and 3(b) which were measured simultaneously during mechanical stretching. We have observed a similar tendency of decrease in slope which is evident from the linear fit of the slope (Table 1) at low q regime of the curve $I \times q^3$ *vs* q and reduction of conductivity with increasing stretching as well.

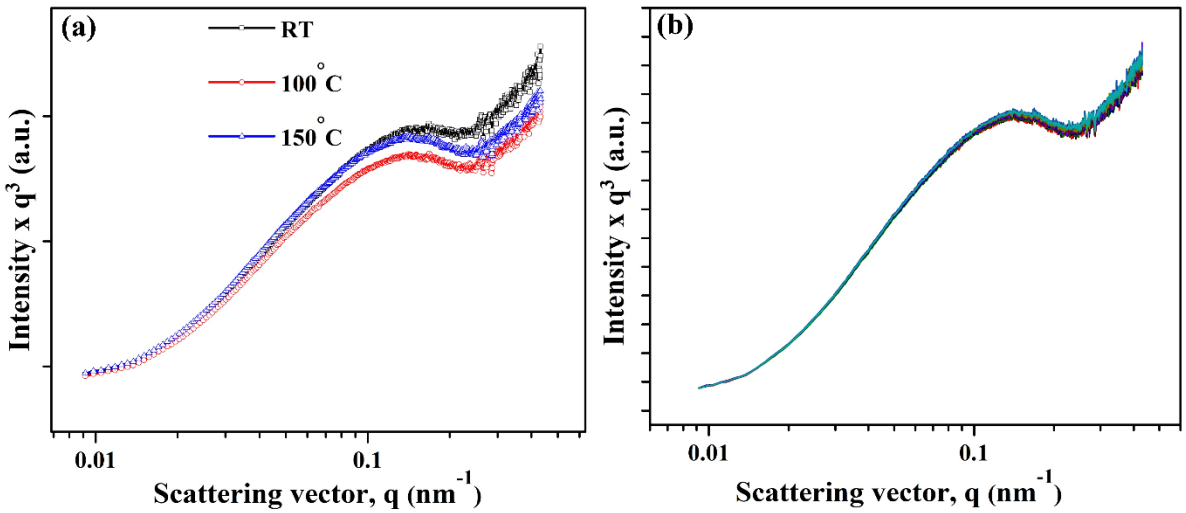

Figure 4: (a) represents the SAXS scattering data for *in-situ* annealed PDMS film with 25 weight percentages of untreated nanotubes at room temperature (black), 100 (red) and 150^0C (blue) respectively where Figure (b) is illustrating the scattering intensity of the same film at 100^0C as a function of time for every 0.5 seconds for 180 seconds.

Furthermore, the role of annealing on conductivity and its correlation with structural changes of nanofillers aggregates have been studied. The provision of *in-situ* heating the film during the measurement of conductivity and USAXS scattering intensity have been made and figure 4(a) shows a comparative scattering profile as a function of temperature using the MWCNT sample of above the percolation threshold. The figure 4(b) is representing the *in-situ* USAXS data of

the same CNT sample at 100°C as a function of time. The conductivity of the film has been found to be increasing systematically with annealing temperature which was then remained constant at a particular temperature for the longer time intervals and is tabulated in Table 2. The resistance values of 3.64, 3.45, 3.33 and 3.13 kΩ were recorded at the temperature of 50°, 70°, 80° and 100°C, the similar type of increase in conductivity with annealing were also reported earlier in polymer/ CNT composite systems.[26-27] This increase in conductivity can be explained in terms of reorganization of network structure of nanofillers at high temperature by the construction of multiple contact regions in nanotubes separated by polymeric chains.[28] To obtain further insight into the structure formation of nanotubes as a function of temperature, the region I of $I \times q^3$ *vs* q plot of USAXS scattering has been studied. It was found that the slope of the curve [Figure 4(a)] has become steeper with the increase of temperature which indicates the decrease in fractal dimensions and the formation of more agglomerates in the matrix. In case of figure 4(b), one could not observe any significant change in scattering profiles measured at 100°C for different time intervals. The negligible change in scattering profile as a function of time confirms no change in fractal dimension, and the size of primary and internal structure of particles are constant with time after reaching a particular temperature. The comparison of change of conductivity with temperature [Figure 4(a)] and as a function time at constant temperature [Figure 4(b)] indicates that the fractal dimensions of nanofillers critically vary with temperature due to the higher crystalline phases of polymers at higher temperature.[29] We have established a clear correlation between conductivity and fractal dimension of nanofillers in the polymer matrix as function of external stimuli like shear stress and temperature.

Table 2. The resistances of the PDMS film with 25 wt% of untreated nanotubes at different temperatures indicating the increase in conductivity with temperature.

Temperature (°C)	Resistance (in kΩ)	Percentage of error
50	3.64	0.10
70	3.45	0.05
80	3.33	0.10
100	3.13	0.153

It is interesting to establish that the change in resistance of both 0D CB and 1D CNT based nanocomposites films can be directly correlated with the change in the fractal dimension of the agglomerates. An increase in the mass fractal dimension of the agglomerates has been resulted in an increase of the resistance for a given concentration of the nanofillers. One may note that with increasing concentrations of the filler above the percolation threshold, the number of percolating paths for conduction channels increases and the resistivity would decrease. Thus, an increase in the percolation threshold upon stretching would result in an increase in the resistivity. The systematic increment in fractal dimension by stretching in both the dimensions of carbon nanofillers may also indicate the dissociation of agglomerations size, which can be attributed for reduced electrical conductivity. We observed that at a high loading beyond the percolation threshold, CNTs are mainly remained as clusters where the surface chemistry of nanotubes and interfacial interactions with polymers govern the geometry of fractal dimensions.[22,30]

We can conclude from our *in-situ* stretching, annealing and conductivity measurement studies that the change in fractal dimensions is the key for change in resistance at cyclic stress of flexible nanocomposite film. Our studies indicate that irreversible change in electrical resistance is developed in conducting elastomers due to increase in agglomerate size which

render the conduction pathways. The metal-like conductivity in polymeric matrices can only be achieved when the fillers are loaded much above the percolation threshold. It has been highlighted that the intermolecular particle-particle interactions of filler networks are important to achieve the long-term cyclic stability of mechanical and conductive properties. Our experimental set-up to record real time scattering data as the function of stress, temperature and conductivity for different loading and filler geometries help us to conclude that just increasing the filler loading beyond the percolation threshold is not enough to get the sustained electrical conductivity, the concerned efforts of filler-filler and filler-matrix interactions to be considered for long-term stability.

Experimental Details

Preparation of PDMS nanocomposites

The carbon black acetylene (Alfa Aesar) based PDMS (SYLGARD^{T}M 184 Silicone Elastomer Kit) nanocomposite films were fabricated by doctor's blade method as reported earlier[31] where the film thickness was maintained at 500µm. The method for the preparation of MWCNT (NANOSHEL, NS6130-06-640) reinforced PDMS has been modified for loading high weight fraction of nanotube in polymer matrix. Nanotubes were first dispersed in the solvent (THF) by sonication for 30 minutes at 2mg/ml concentration and then PDMS were introduced into the dispersed medium.[32] The PDMS was mixed with the CNTs under stirring and the solvent were removed by reduced pressure distillation. A few drops of n-decane (Sigma Aldrich) were added into the CNT ink to reduce the viscosity using vacuum speed mixer and the 500µm of nanocomposite film were prepared by doctor's blade method with slow curing. The covalent functionalization of MWCNTs were followed by our established process[23] and for non-covalent functionalization, ionic liquid [1-ethyl-3-methylimidazolium bis(trifluoromethanesulfonic)] was used.

Combined In-situ Ultra-Small Angle X-ray Scattering (USAXS) and conductivity measurements

In situ USAXS measurements during mechanical stretching in a controlled way were carried out at P03 beamline of PETRA III storage ring at DESY, Hamburg, Germany.[33] The X-ray energy was 11.8 keV corresponding to the wavelength of 0.105 nm and the beam size was 70 × 53 μm^2 (horizontal × vertical dimension). The scattered intensity was measured using a 2D LAMBDA 750k detector (X-Spectrum, Hamburg, Germany) with a pixel size of 55 μm positioned at a distance of (9550±1) mm from the sample. Such an ultra-small q range provides the details about the micro and nano scale structures in the sample. The intensity is obtained as a function of q which is given as $q = \frac{4\pi}{\lambda} sin\theta$, with λ being the wavelength of the X-rays and θ being half of the scattering angle.

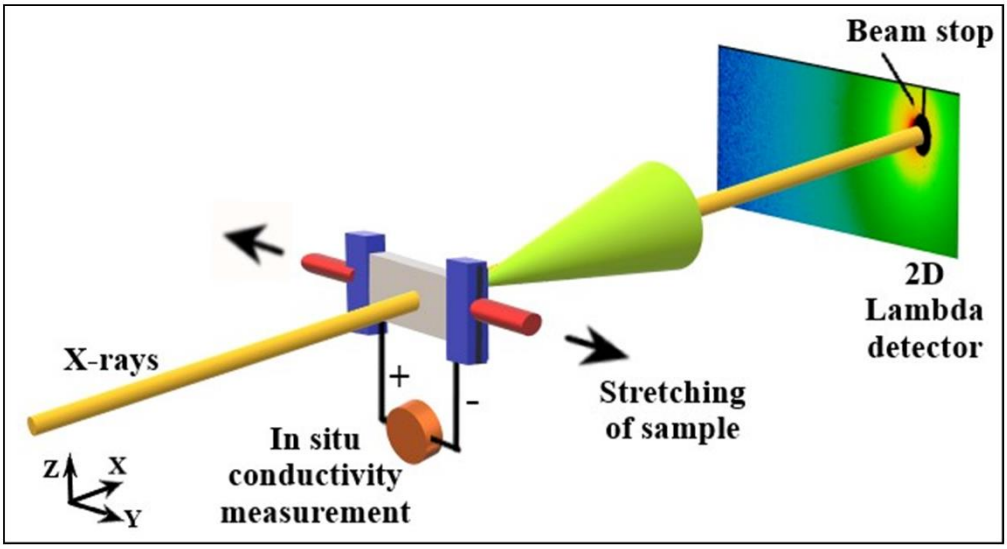

Scheme 1. Representation for the combined *in situ* USAXS and conductivity measurement.

The samples were subjected to a strain of 5, 10, 20 and 30% from their nominal length of 20 mm at a rate of 1 mm/second and SAXS data were recorded for each 0.5 seconds. More technical details about the mechanical stretching device can be found in Ref 34. To extract the variation of X-ray scattering intensity as a function of scattering vector q from 2D USAXS plots, the DPDAK software suite has been used.[35] The data were integrated azimuthally at

different positions from the beam centre on the 2D detector and background subtracted following known procedures from literature.[36]

The conductivity measurements have been done simultaneously during the stretching to understand variation in transport properties under the strain. Schematic of *in situ* conductivity along with USAXS during mechanical stretching has been shown in scheme 1. A constant potential of 20 V was applied along the length of the polymer sample with dimensions 20 × 10 × 1 mm (l × w × t) and measured current using a multimeter (Keithley make).

Acknowledgements

Most of the authors of this scientific contribution are mentored or greatly supported by Professor Dr. (Acad.) Eduard Arzt. They all would like to thank him profoundly for his exemplary encouragement and wish him all the very best on the special occasion of superannuating from INM, Saarbrucken, Germany. One of the authors (DR) specially would like to express on this occasion that he feels indebted to Professor Eduard Artz for hosting him at INM to conduct some of these scientific studies. Hence, this work is specially dedicated to him for not only supporting us all, but many such researchers and collaborations with many international laboratories and institutions. He also feels greatly obliged to Professor Tobias Kraus and his fellow associates in Leibniz Institute for New Materials (INM) for making his stay most rewarding, which was made possible by a liberal financial support by a Fellowship under German Academic Exchange Programme from DAAD, Germany. Dr. Roy also wants to place on record his heartfelt thanks to the Directors, DMSRDE; DGs, NSM of DRDO; and, Chairmen, DRDO for their constant encouragement and exemplary support to the nanomaterials research at DMSRDE, Kanpur, India and also for their permission for his sabbatical at INM.

The major portion of this research work have been carried out at the light source PETRA III, DESY, a member of the Helmholtz Association (HGF), Germany; the provision of this facility

is gratefully acknowledged. Finally, the travel financial support provided to SKV and AG by Department of Science and Technology (DST), Government of India within the framework of the India-DESY collaboration too is highly acknowledged. Vaishnav acknowledges the fellowship from the DRDO under the project TR/0569/CARS-135. All the authors thank all their respective academic collaborators for their support and suggestions/advice they received from time to time.

References

(1) Wang, C.; Xia, K.; Wang, H.; Liang, X.; Yin, Z.; Zhang, Y. Advanced carbon for flexible and wearable electronics. *Adv. Mater.* **2018**, 31.

(2) Gao, W.; Ota, H.; Kiriya, D.; Takei, K.; Javey. Flexible electronics toward wearable sensing. *Acc. Chem. Res.* **2019**, 52, 523.

(3) Yin, R.; Wang, D.; Zhao, S.; Lou, Z.; Shen, G. Wearable sensors-enabled human-machine interaction systems: from design to application. *Adv. Func. Mater.* **2021**, 31, 2008936.

(4) Kim, K. K.; Suh, Y.; Ko, S. H. Smart stretchable electronics for advanced human-machine interface. *Adv. Intell. Syst.* **2021**, 3, 2000157.

(5) Chun, S.; Son, W.; Kim, D. W.; Lee, J.; Min, H.; Jung, H.; Kwon, D.; Kim, A. H.; Kim, Y. J.; Lim, S. K.; et.al. Water-resistant and skin-adhesive wearable electronics using graphene fabric sensor with octopus-inspired microsuckers. *ACS Appl. Mater. Interfaces* **2019**, 11, 16951.

(6) Song, Y.; Mukasa, D.; Zhang, H.; Gao, W. Self-powered wearable biosensors. *Acc. Mater. Res.* **2021**, 2, 184.

(7) Amjadi, M.; Pichitpajongkit, A.; Lee, S.; Ryu, S.; Park, I. Highly stretchable and sensitive strain sensor based on silver nanowire-elastomer nanocomposite. *ACS Nano* **2014**, 8, 5154.

(8) Liu, C. Recent developments in polymer MEMS. *Adv. Mater.* **2007**, 19, 3783.

(9) Natarajan, T. S.; Eshwaran, S. B.; Stöckelhuber, K. Werner; Wießner, S.; Pötschke, P.; Heinrich, G.; Das, A. Strong strain sensing performance of natural rubber nanocomposites. *ACS Appl. Mater. Interfaces* **2017**, 9, 4860.

(10) Pan, Y.; Liu, X.; Kaschta, J.; Hao, X.; Liu, C.; Schubert, D. W. Viscoelastic and electrical behavior of poly(methyl methacrylate)/carbon black composites prior to and after annealing. *Polymer* **2017**, 113, 34

(11) Tan, H. W.; Choong, Y. Y. C.; Kuo, C. N.; Low, H. Y.; Chua, C. K. 3D printed electronics: processes, materials and future trends. *Prog. Mater. Sci.* **2022**, 127, 100945.

(12) Yan, T.; Wang, Z.; Pan, Z. J. Flexible strain sensors fabricated using carbon-based nanomaterials: A review. *Curr. Opin. Solid. State Mater. Sci.* **2018**, 22, 213.

(13) Liu, X.; Krückel, J.; Zheng, G.; Schubert, D. W. Electrical conductivity behaviour of sheared poly(methyl methacrylate)/carbon black composites. *Compos. Sci. Technol.* **2014**, 100, 99

(14) T. Khan; M.S. Irfan; M. Ali; Y. Dong; S. Ramakrishna; R. Umer. Insights to low electrical percolation thresholds of carbon-based polypropylene nanocomposites. *Carbon* **2021**, 176, 602.

(15) Xiang F; Schneider K; Schwartzkopf M; Heinrich G. Competition between strain-induced crystallization and cavitation at the crack tip of unfilled and carbon black filled natural rubber. *Macromolecules* **2022**, 55, 10682.

(16) Voupette, F.; Zhang, L.; Kuttich, B.; Chumakov, A..; Roth, S. V.; González-García, L.; Kraus, T.; Schilling, T. Percolation of rigid fractal Carbon black aggregates. *J. Chem. Phys.* **2021**, 155, 124902.

(17) Jäger, K. M.; McQueen, D. H. Fractal agglomerates and electrical conductivity in carbon black polymer composites. *Polymer* **2001**, 42, 9575.

(18) Cherny, A. Y.; Anitas, E. M.; Osipov, V. A.; Kuklin, A. I. The structure of deterministic mass and surface fractals: theory and methods of analyzing small-angle scattering data. *Phys. Chem. Chem. Phys.* **2019**, 21, 12748.

(19) Kohjiya, S.; Katoh, A.; Suda, T.; Shimanuki, J.; Ikeda, Y. Visualisation of carbon black networks in rubbery matrix by skeletonisation of 3D-TEM image. *Polymer* **2006**, 47, 3298.

(20) Norkhairunnisa, M; Azizan, A; Mariatti, M; Ismail, H; Sim, L. Thermal stability and electrical behavior of polydimethylsiloxane nanocomposites with carbon nanotubes and carbon black fillers. *J. Compos. Mater.* **2012**, 46, 903.

(21) Bauhofer, W.; Kovacs, J. Z. A review and analysis of electrical percolation in carbon nanotube polymer composites. *Compos. Sci. Technol.* **2009**, 69, 1486.

(22) Oseli, A.; Vesel, A.; Žagar, E.; Perše, L. S. Mechanisms of single-walled carbon nanotube network formation and its configuration in polymer-based nanocomposites. *Macromolecules* **2021**, 54, 3334.

(23) Hudda, A.; Singh, S.; Tiwari, S.; Kumar, H.; Vesh, A.; Imamuddin, Md.; Roy, D.; Prasad, N. E. Unravelling the role of nanofillers towards the stability of polymer matrix composite in marine environment. *Adv. Compos. Mater.* **2023**, 32, 268.

(24) Wang, Y.; Iqbal, Z.; Mitra, S. Rapidly functionalized, water-dispersed carbon nanotubes at high concentration. *J. Am. Chem. Soc.* **2006**, 128, 95.

(25) Beigbeder, A.; Linares, M.; Devalckenaere, M.; Degée, P.; Claes, M.; Beljonne, D.; Lazzaroni, R.; Duboi, P. CH-π interactions as the driving force for silicone-based nanocomposites with exceptional properties. *Adv. Mater.* **2008**, 20, 1003.

(26) Mohiuddin, M.; Hoa, S.V. Temperature dependent electrical conductivity of CNT-PEEK composites. *Compos. Sci. Technol.* **2011**, 72, 21.

(27) Simsek; Y.; Ozyuzer, L.; Seyhan, A. T.; Tanoglu, M.; Schulte, K. Temperature dependence of electrical conductivity in double-wall and multi-wall carbon nanotube/polyester nanocomposites. *J. Mater. Sci.* 2007, 42, 9689.

(28) Kędzierski, K.; Rytel, K.; Barszcz, B.; Gronostaj, A.; Majchrzycki, L.; Wróbel, D. On the temperature dependent electrical resistivity of CNT layers in view of variable range hopping models. *Org. Electron.* **2017**, 43, 253.

(29) Ingo Alig; Dirk Lellinger; Sergej M. Dudkin; Petra Pötschke. Conductivity spectroscopy on melt processed polypropylene–multiwalled carbon nanotube composites: Recovery after shear and crystallization. *Polymer* **2007**, 48, 1020.

(30) Zhang, M.; Zhang, W.; Jiang, N.; Futaba, D. N.; Xu, M. A general strategy for optimizing composite properties by evaluating the interfacial surface area of dispersed carbon nanotubes by fractal dimension. *Carbon* **2019**, 154, 457.

(31) Söz, C. K.; Yilgör, E.; Yilgör, I. Influence of the coating method on the formation of superhydrophobic silicone–urea surfaces modified with fumed silica nanoparticles. *Prog. Org. Coat.* **2015**, 84, 143.

(32) Zheng, Y.; Li, Y.; Li, Z.; Wang, Y.; Dai, K.; Zheng, G.; Liu, C.; Shen, C. The effect of filler dimensionality on the electromechanical performance of polydimethylsiloxane based conductive nanocomposites for flexible strain sensors. *Compos. Sci. Technol.* **2017**, 139, 64.

(33) Buffet, A.; A. Rothkirch; R. Döhrmann; Yu, S.; V. Körstgens; M. M. Abdul Kashem; J. Perlich; G. Herzog; M. Schwartzkopf; R. Gehrke; P. Müller-Buschbaum; S. V. Roth. P03, the microfocus and nanofocus X-ray scattering (MiNaXS) beamline of PETRA III storage ring: the microfocus endstation. *J. Synchrotron Rad.* **2012**, 19, 674.

(34) E Euchler; A K Sambale; K Schneider; K Uhlig; R Boldt; M Stommel; M Schwartkopf; A Rothkirch; S V Roth. Beamline-implemented stretching devices for in situ X-ray scattering experiments. *J. Phys. Conf. Ser.* **2022**, 2380, 012109.

(35) Benecke, G.; Wagermaier, W.; Li, C.; Schwartzkopf, M.; Flucke, G.; Hoerth, R.; Zizak, I.; Burghammer, M.; Metwalli, E.; Müller-Buschbaum, P. et. al. A customizable software for fast reduction and analysis of large X-ray scattering data sets: applications of the new DPDAK package to small-angle X-ray scattering and grazing-incidence small-angle X-ray scattering. *J. Appl. Crystallogr.* **2014**, 47, 1797.

(36) Pauw, B. R.; Smith, A. J.; Snow, T.; Terrill, N. J.; Thünemann, A. F. The modular small-angle X-ray scattering data correction sequence. *J. Appl. Crystallogr.* **2017**, 50, 1800.